# Optical Rotation of Dilute Aqueous Xanthan Solutions at Elevated Hydrostatic Pressure

B. T. STOKKE,* K. D. KNUDSEN, O. SMIDSRØD, and A. ELGSAETER

Norwegian Biopolymer Laboratory, Department of Physics and Mathematics, Norwegian Institute of Technology, University of Trondheim, 7034 Trondheim, Norway

SYNOPSIS

The optical rotation of dilute aqueous xanthan solutions of ultrasonically depolymerized xanthan have been measured in the pressure range from 0.1 to 50 MPa. This was achieved using a high-pressure cell in a spectropolarimeter of original design. The conformational melting temperature $T_m$ of xanthan was found to decrease with increasing pressure. The pressure coefficients of the melting temperature at constant ionic strengths, $I$, was found to be $(\Delta T_m/\Delta p)_I = -(9.5 \pm 4.0)\ 10^{-8}$ K Pa$^{-1}$ and $(\Delta T_m/\Delta p)_I = -(20 \pm 10)\ 10^{-8}$ K Pa$^{-1}$ for solution ionic strengths of 10 m$M$ NaCl and 25 m$M$ NaCl, respectively. The largest shift in $T_m$ of xanthan for an increase in hydrostatic pressure from 0.1 to 50 MPa is less than $-10$ K. The observed decrease in conformational transition temperature can have significant implications when xanthan is used in polymer or micellar flooding processes in high-salinity, high-temperature oil reservoirs where the reservoir temperature is close to the structural transition temperature at ambient pressure.

## INTRODUCTION

The successful application of xanthan and other polymers in industrial processes in general, and as mobility controlling agent in chemical flooding for enhanced oil recovery (EOR) in particular, require that the polymers satisfy the criteria of the process. The demands put on a mobility controlling agent to be applied in high-temperature, high-salinity reservoirs range from having good injectivity and high viscosity at flooding shear rates at the reservoir temperature to being stable against mechanical, biological, chemical, and thermal degradation both during injection and over the residence period in the reservoir. There should further be minimal adsorption to the reservoir rock, thereby preventing efficiency loss as the slug is moving ahead. In addition, the relatively high hydrostatic pressure found in many reservoirs should have no adverse effects on these properties.

The laboratory evaluation of polymers being considered for viscosifying fluids injected in order to obtain adequate mobility control has addressed most of the requirements mentioned above.[1,2] However, there are virtually none addressing the effect of hydrostatic pressure on the polymer properties. For instance, the thermal stability under temperature conditions mimicking those in the reservoir have shown that the application of xanthan biopolymers is limited to reservoirs below about 90°C.[1,3,4] From the thermal stability tests of xanthan, it is also well documented that the chiroptically referred conformational transition has a significant effect on the thermal stability. We use the term thermal stability to represent resistance toward all mechanisms leading to breakdown of the covalent structure at high temperature whatever the specific mechanism (e.g., acid- or base-catalyzed, free radical mechanism). This thermal stability is to be distinguished from the structural stability of the biopolymer, which is used to designate the stability of the ordered conformation of xanthan against melting. For high-temperature and high-salinity conditions favoring the ordered conformation, the characteristic degradation rate is reduced five times or more compared to that of the disordered conformation.[5,6] It is therefore essential to maintain the ordered conformation during the flooding process to ensure the thermal stability of xanthan.

In the literature it is documented that ordered macromolecules may change their structure due to

* To whom correspondence should be addressed.

Journal of Applied Polymer Science, Vol. 42, 2063–2071 (1991)
 CCC 0021-8995/91/072063-09$04.00

an applied hydrostatic pressure. In the case of DNA, hydrostatic pressure is reported to stabilize or destabilize its double-helical structure depending on the source of the material.[7] Because of the potential economical risks of a lowering of the conformational melting temperature of xanthan as a result of increasing the hydrostatic pressure, and thereby inducing the inherent thermally and enzymatically[8] less stable conformation, the effect of hydrostatic pressure on xanthan is of utmost importance in many applications. In addition to this issue associated with the application of xanthan in high-pressure, high-temperature oil reservoirs, effects of pressure on the conformational transition yield information on the thermodynamic parameters characterizing the transition.[9,10]

In the following, our strategy to measure optical rotation at pressures up to about 50 MPa for temperatures approaching 100°C and the application of this strategy to the study of pressure effects on dilute aqueous xanthan solutions will be described. The hardware designed to address the high-pressure optical activity is based on having light source, analyzer, and detector all at ambient pressure, while the liquid is pressurized. As a safety precaution, we pressurize only liquid and no gas, thereby minimizing the volume change due to the pressure change.

To obtain good signal-to-noise ratio and still keep the viscosity sufficiently low to avoid problems during filling of the cell, we routinely used low molecular weight xanthan obtained by ultrasonic degradation. The melting curves of the ordered conformation are obtained for xanthan in aqueous solution with a total ionic strength from 1 to 100 m$M$ as a function of hydrostatic pressure.

## EXPERIMENTAL

### Design of a High-Pressure Spectropolarimeter

Figure 1 shows a schematic drawing of the main components of the high-pressure spectropolarimeter. Most of the components in the light path are analogous to those in commercial instruments: a light source (450 W Xenon lamp, Osram XBO 450W/1), a wavelength selecting grating-type monochromator (Jobin-Yvn H.20UV), a polarizer (Glan Thompson polarizer Type II, extinction coefficient better $10^{-7}$), an analyzer (same type as polarizer), and a light-detecting device (Photomultiplier EMI9558QF). The sample cell body is mechanically designed to sustain pressures up to 200 MPa. It is machined from a corrosion-resistant Ni—Cu alloy (Monel 400, Wiggin Alloys). The entry and exit windows are made of fused quartz, custom made by Helma in quartz quality 665-QS Suprasil, with adequate transmittance for wavelengths, $\lambda$, from about 200–800 nm. These windows are sealed to their support, designed according to Claesson and Hayward[11] using Apiezon vacuum grease. The window supports are sealed to the cell housing using two O-rings (Viton) and locked with a threaded ring.

The sample entrance and exit holes are located near the two windows; the entrance is from below and exit on top so that the solution should remove the air in the sample cell when filled. However, in a number of initial trials, it proved difficult to fill the cell completely. Two extra channels were made from the top to facilitate easy removal of remaining air bubbles.

The temperature in the cell was controlled by circulating water under thermostat control (Haake D8-G) through six interconnected paraxial holes ($\phi$8 mm). The hydrostatic pressure exerted on the sample was controlled by a pressure-generating system through high-pressure tubing (High-Pressure Equipment 316 S.S., 1/8 in. OD, 30 kpsi [200 MPa] rating) sealed to the cell by a matching fitting. The pressure was generated by a hand pump (High-Pressure Equipment model 37-6-30) modified to be controlled by a computer-controlled stepping motor. The pressurizing fluid (glycerol) was separated from the sample using a separator. The pressure was

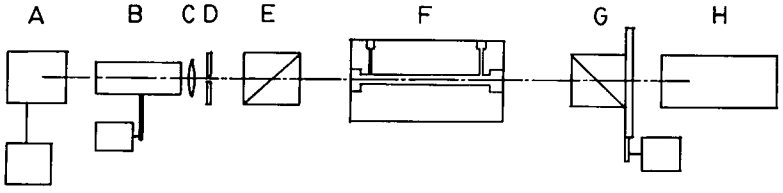


**Figure 1** Schematic drawing showing the main components in the light path of the high-pressure spectropolarimeter: light source (A), stepping motor-controlled monochromator (B), lens (C), aperture (D), polarizer (E), high-pressure sample cell (F), stepping motor-controlled analyzer (G), and photomultiplier tube (H). The optical path is depicted as (— - —).

monitored on the pressurizing fluid side of the separator using a mechanical gauge (High-Pressure Equipment 6PG20) and on the sample side of the separator, i.e., in the high-pressure cell where the measurement took place by means of an electronic transducer (Hottinger Baldwin P3MA). Details in the polarizer assembly, analyzer assembly, and light-detection system are given elsewhere.[12]

The high-pressure spectropolarimeter is set up with complete computer control of all the experimental parameters such as temperature, temperature scan, hydrostatic pressure, wavelength ($\lambda$), wavelength scan, as well as data collection parameters. This is implemented by an operator-designed control file that controls the sequence of actions being invoked. There is no time limit in the length of a run. However, for practical reasons, such as inspection of data, modification of parameters, etc., we limited ourselves to runs not exceeding 24 h. In addition to the software controlling the instrument operation and data collection, we have developed software for data analysis, i.e., specific optical rotation vs. temperature and pressure, Moffit plots, etc., making use of the same control files.

## Instrument Performance

The accuracy of the measured angle of rotation, $\alpha$, for a given solution was experimentally determined to 2 mdeg (SD, N = 20) when the data collection mode is selected with a long integration time ($\sim$ 2 s). For shorter integration times, the accuracy is reduced and is recommended only when the measured optical rotation is large ($>$ 1 deg).

The temperature of the thermostatically controlled circulating water could be maintained within $\pm$0.1°C inside the thermostat bath. In the present application, the circulating water was found to be able to yield and maintain a stable temperature plateau ($\pm$0.1°C uncertainty) inside the sample chamber within 10 min after a 5°C temperature change. The time-constant in the transition from the disordered to the ordered conformation of xanthan is reported to be on the order of 1–3 s (Ref. 13) to 0.01–10 s (Ref. 14). Optical rotation measurements after a thermal equilibration of 10 min are therefore adequate to obtain conformational equilibrium at each temperature in a temperature scan.

There have been several reports on the strain-induced birefringence in entrance and exit windows in similar high-pressure cells due to the increased hydrostatic pressure.[15,16] We observed similar phenomena. The significance of this is that the lower wavelength limit accessible for the specific optical rotation increases as the hydrostatic pressure increases. Although this is a limitation, the melting profiles for dilute xanthan solutions can still be obtained. This is so because the optical rotation of the last dialysis solution (ideally used to determine the baseline) or distilled water at one given pressure did not change within the temperature range from 10 to 85°C, whereas a sigmoidal increase was observed for the xanthan solutions. The sigmoidal increase is therefore due to the polysaccharide.

The specific optical rotation, $[\alpha]$, of a 1% sucrose solution was measured in the high-pressure spectropolarimeter to within 1% of the tabulated[17] at 0.1 MPa. The wavelength range was from $\lambda$ = 350 nm to $\lambda$ = 700 nm, and no systematic deviations as a function of wavelength from the tabulated was evident. We observed no significant effect on $[\alpha]$ for sucrose for hydrostatic pressure up to 50 MPa, which is in line with earlier reports.[18] However, due to the strain-induced birefringence in the windows, the lower wavelength limit for carrying out measurements increased to about 500 nm at 50 MPa.

## Preparation of Aqueous Xanthan Solutions

Powdered xanthan (Kelzan XCD, Kelco, a division of Merck Inc., San Diego, CA) was dispersed at a concentration of 2–3 mg/mL in 10 m*M* NaCl and stirred at room temperature overnight. The polymer was depolymerized by ultrasound irradiation (Braun Labsonic 1510) in batches of 300 mL, for 3 $\times$ 10 min at a power of 300 W. The solutions were kept on ice during the ultrasound exposure to avoid large heating effects. The solution was then centrifuged at 200,000 *g* (Beckman 50 Ti, 45,000 rpm) for 60 min, and the supernatant dialyzed against 3–4 $\times$ 1000 mL aqueous sodium chloride solution with the desired ionic strength (1–100 m*M*). The polymer concentration was determined as the total carbohydrate remaining in the dialysis bag after final change of dialysis solution using a colorimetric method.[19]

The samples were then degassed and loaded in the high-pressure cell of the spectropolarimeter at 20°C. The optical rotation is measured, in principle, relative to that of the last dialysis solution. However, both because the optical rotation of salt solutions differ insignificantly from that of distilled water and because only the relative change of the optical rotation is used to assign regions of ordered and disordered conformations for polysaccharides, we here report only on $\alpha$ where the measured value of distilled water was used as a baseline. Measurements were carried out either as wavelength series at constant

pressure for temperature scans covering the xanthan conformational melting temperature at the particular ionic strength or as λ-series at constant temperature and varying the pressure. The temperature melting curves were determined for hydrostatic pressures from 0.1 to 50 MPa.

## RESULTS AND DISCUSSION

### Optical Rotation

Figure 2 shows the absolute optical rotation for ultrasonically depolymerized xanthan in 10 m*M* NaCl vs. the temperature for hydrostatic pressures of 0.1 MPa (λ = 410 nm), 24.9 MPa (λ = 470 nm), and 49.3 MPa (λ = 540 nm). The present sample at all pressures shows the characteristic sigmoidal decrease in absolute value of specific optical rotation on increasing temperature as has been reported previously for studies at 0.1 MPa.[20-24] When the hydrostatic pressure increases, the midpoint of the sigmoidal increase is significantly shifted toward lower temperature. The sigmoidal increase of $\alpha$ is used to qualitatively ascertain regions of ($p$, $T$, $I$) where the ordered or disordered conformation is prevailing.[23,24] Only recently has the quantitative value of the specific rotation [$\alpha$] been given a semiempiric interpretation.[25] We will follow the qualitative practice of using the optical signal to assign ordered and disordered domains of the xanthan conformation in ($p$, $T$, $I$) space.

### Determination of Conformational Transition Temperature

The temperature at which [$\alpha$] is halfway between the low-temperature and the high-temperature plateaus is commonly referred to as the conformational melting or transition temperature, $T_m$. To obtain quantitative estimates of $T_m$ based on the complete temperature scan rather than by means of a graphical method, we suggest to use the helix-coil transition theory. The applicability of this theory to the conformational ordering of xanthan has previously been demonstrated with the interpretation that the ordering is within each single-stranded xanthan chain.[13] However, the applicability of the helix-coil transition theory is not limited to the single-stranded case. Because we previously have obtained evidence that there could be a transition in strandedness on going through the chiroptically recorded conformational transition,[26,27] we assign the perfectly matched double-stranded structure to the chiroptically referred ordered conformation and the partly or fully dissociated structure to the disordered conformation. The equilibrium or so-called propagation constant $s$ associated with increasing the length of sequence of ordered ($o$) elements in an array of disordered $d$ elements is given as (see, for instance, Cantor and Schimmel[28]):

$$s = \frac{..ddooodd..}{..ddooddd..} \tag{1}$$

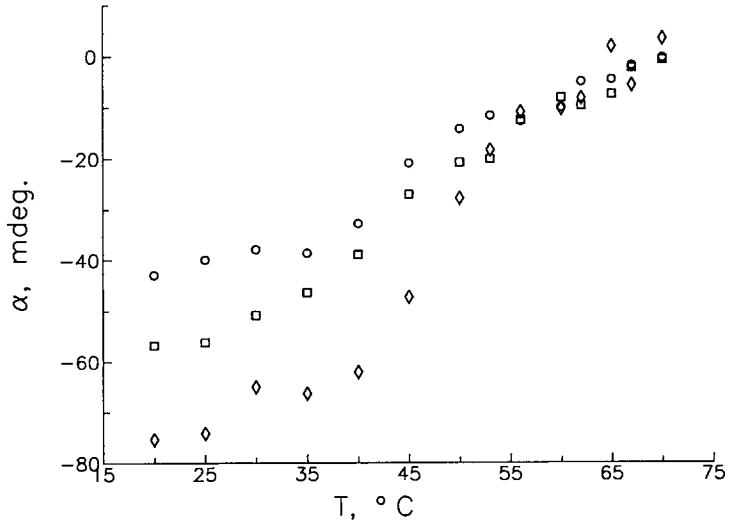


**Figure 2** Absolute optical rotation of xanthan solutions vs. temperature for $c$ = 1.7 mg/mL in 10 m*M* NaCl at $p$ = 0.1 MPa, λ = 410 nm (◇); $p$ = 24.9 MPa, λ = 470 nm (□); and $p$ = 49.3 MPa, λ = 540 nm (○).

and the additional penalty $\sigma$, cooperativity parameter, associated with initiating such a sequence is given by

$$\sigma s = \frac{..dddoddd...}{..ddddddd...} \quad (2)$$

Because our previous results on samples prepared analogously[26,27] suggests that the ordered conformation of xanthan is double-stranded, we identify the nucleation parameter as the entropy loss from bringing two chains together in such a way that the pairing propagation [equilibrium constant $s$, eq. (1)] can proceed. Based on these simple equilibria, the partition function for all sequence lengths can be constructed and the average length of $o$-sequences relative to that of the total chain length, i.e., the fractional order $\theta$, is given by eq. (3)[28]:

$$\theta(s) = 0.5\frac{s}{\lambda_1} \cdot \left(1 + \frac{s - 1 + 2\sigma}{((1-s)^2 + 4\sigma s)^{1/2}}\right) \quad (3)$$

where $\lambda_1$ is an eigenvalue in the statistical weight matrix and is given by

$$\lambda_1 = 0.5[1 + s + ((1-s)^2 + 4\sigma s)^{1/2}] \quad (4)$$

The propagation constant $s$ is specified at the actual temperature $T$ relative to $T_m$ by an integrated van't Hof's relation:

$$\ln s = \frac{\Delta H'}{R} \cdot \left(\frac{1}{T_m} - \frac{1}{T}\right) \quad (5)$$

where $\Delta H' = -\Delta H$, and $\Delta H$ is the calorimetric enthalpy per repeating unit in the transition, and $R$, the molar gas constant. At $T = T_m$, $s = 1$ and $\theta$ ($s = 1$) = 1/2. By applying this theory to extract $T_m$ from the experimental data, we assigned $\theta = 1$ to the low-temperature plateau and $\theta = 0$ to the high-temperature plateau. From an initial guess of the melting temperature, $T_m$ is estimated by minimizing the sum of squares between the predicted $\theta$ and that deduced from the experimental data using a simplex algorithm (nonlinear regression).[29] In this procedure, $\sigma$ and $T_m$ are estimated simultaneously provided that $\Delta H$ is specified (set to literature value). Alternatively, $\Delta H$ could be estimated when it was assumed that $\sigma$ was known and an actual value of $\sigma$ supplied to the simplex algorithm. We found that parameters $\sigma$ and $\Delta H$ could not be uniquely estimated simultaneously. The estimated value of $\sigma$ from the data depends on the actual value of $\Delta H$, but $T_m$ could be determined with an accuracy of $\pm 0.05$ K depending on the actual value of $\Delta H$ or $\sigma$ when the alternative procedure was used. The uncertainties using this approach to estimate $T_m$ lie mainly in the assignment of $\alpha$-levels for the ordered and disordered conformations. Including estimation of these $\alpha$-levels in the simplex algorithm did not yield numerical stable solutions in all cases and was therefore not incorporated in the final estimates. The uncertainties in the estimates of $T_m$ using this approach are on the order of 0.5–1.0°C for most cases, but are found to approach 2°C for data where the low- and high- temperature plateaus were not clearly distinguishable (Table I).

Figure 3 shows the specific optical rotation data of Figure 2 converted to fractional order data, $\theta$, assigning the high- and low-temperature regions as described. The theoretical curves for the three pressures calculated from the estimated values of $T_m$ and $\sigma$ ($\Delta H$ = 7.1 kJ/mol[13]) conform with the data for all the temperatures, and largest deviation between experiment and theory is 0.1 order units, which corresponds to 7 mdeg, whereas 60% of the residuals are within 0.03 in fractional order, with no systematic dependence upon the actual temperature. This corresponds well with the experimental uncertainty determined independently (±2 mdeg). Table I summarizes the transition data obtained at different pressures and solution ionic strengths. The estimated melting temperatures for the ultrasonically depolymerized xanthan at an ionic strength of 10 m$M$ are $T_m$ = 49.3 ± 1.5°C (combination of the two tabulated values) at $p$ = 0.1 MPa, decreasing to $T_m$ = 46.7 ± 1°C at 24.9 MPa, and further decreasing to $T_m$ = 43 ± 1°C at $p$ = 49.3 MPa. A systematic decrease of the melting temperature is also observed in 25 m$M$ NaCl, but the experimental uncertainties are larger. The slope of the transition at $T_m$ is also reported. This slope is related to the enthalpy of the transition and the cooperativity parameter $\sigma$[18]:

$$\left(\frac{\partial\theta}{\partial T}\right)_{s=1} = \frac{-\Delta H}{4RT_m^2\sigma^{1/2}} \quad (6)$$

The change in fractional order at $T_m$ are all within −0.030/K to −0.078/K (Table I), and the uncertainties in these estimates hide almost any possible systematic dependence. Only for $I$ = 10 m$M$, there is an indication that there is a systematic decrease in this parameter for increasing pressure and thus the transition steepness upon temperature change decreases with increasing pressure. A more pronounced decrease in the transition steepness ($\partial\theta$/

**Table I Melting Temperature, $T_m$, Cooperativity Parameter, $\sigma$, and Steepness of Conformational Transition $(\Delta\theta/\Delta T)_{T=T_m}$, at Different Ionic Strengths, $I$ and Hydrostatic Pressure, $p$**

| $I$ (m$M$) | $p \cdot 10^{-5}$ (Pa) | $T_m$ (°C) | $10^3/T_m$ ($K^{-1}$) | $\sigma \cdot 10^3$ | $(\Delta\theta/\Delta T)_{T=T_m}$ ($K^{-1}$) |
|---|---|---|---|---|---|
| 25 | 1 | 58.5 ± 2.0 | 3.015 | 3.0 | −0.030 ± 0.010 |
| | 109 | 54.3 ± 0.9 | 3.054 | 3.0 | −0.038 ± 0.008 |
| | 214 | 57.5 ± 1.0 | 3.024 | 1.2 | −0.053 ± 0.006 |
| | 319 | 52.0 ± 1.0 | 3.075 | 1.8 | −0.046 ± 0.005 |
| | 493 | 47.0 ± 0.9 | 3.123 | 3.0 | −0.040 ± 0.005 |
| 15 | 1 | 52.5 ± 1.3 | 3.071 | 1.9 | −0.045 ± 0.006 |
| 10 | 1 | 50.5 ± 1.1 | 3.090 | 2.0 | −0.052 ± 0.006 |
| | 1 | 48.0 ± 0.5 | 3.114 | 1.3 | −0.058 ± 0.007 |
| | 144 | 52.5 ± 0.9 | 3.071 | 1.1 | −0.062 ± 0.017 |
| | 249 | 46.3 ± 0.6 | 3.128 | 1.2 | −0.049 ± 0.007 |
| | 249 | 47.0 ± 1.0 | 3.123 | | |
| | 319 | 46.0 ± 0.9 | 3.133 | | |
| | 353 | 46.1 ± 1.2 | 3.135 | 2.1 | −0.045 ± 0.004 |
| | 459 | 45.2 ± 1.0 | 3.151 | 2.0 | −0.043 ± 0.004 |
| | 493 | 43.0 ± 1.0 | 3.163 | | |
| 7.5 | 1 | 47.4 ± 1.0 | 3.12 | 1.0 | −0.078 ± 0.010 |
| | 144 | 46.0 ± 1.1 | 3.19 | 1.5 | −0.054 ± 0.004 |
| | 249 | 46.3 ± 0.9 | 3.128 | 1.5 | −0.052 ± 0.004 |
| 5 | 1 | 44.0 ± 0.9 | 3.153 | 1.5 | −0.049 ± 0.010 |

$\partial T)_{s=1}$ is reported for the temperature-induced helix formation of poly(γ-benzylglutamate).[18]

Equation (6) relates the experimentally determined $(\Delta\theta/\Delta T)$ to $\Delta H$, $T_m$, and $\sigma$ and also supports the finding that $\Delta H$ and $\sigma$ could not be determined independently at the same time. Experimentally determined values of $(\Delta\theta/\Delta T)_{s=1}$ provide estimates of $\Delta H/\sigma^{1/2}$ [eq. (6)]. The two latter parameters can-

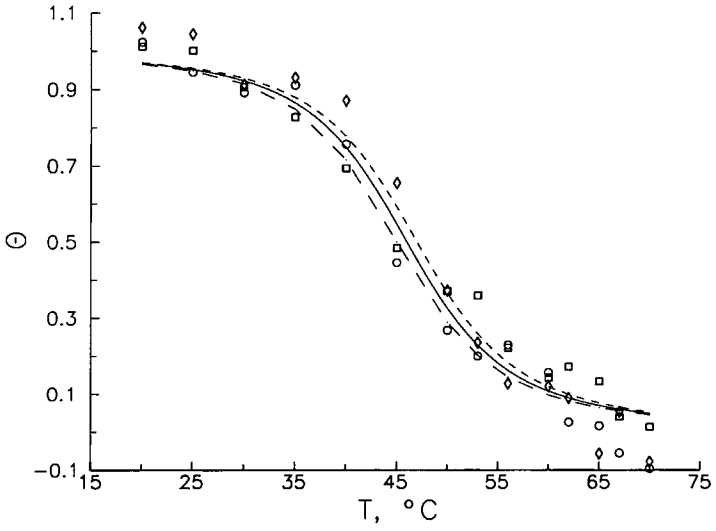


**Figure 3** Estimated $\theta(T)$ from optical rotation data of xanthan solutions vs. temperature. Actual data points are for $c$ = 1.7 mg/mL in 10 m$M$ NaCl at $p$ = 0.1 MPa, λ = 410 nm (◇, -----); $p$ = 24.9 MPa, λ = 470 nm (□, ——); and $p$ = 49.3 MPa, λ = 540 nm (○, — — — —), and the least-squares adjusted curves as indicated with the pressure mark.

not be separated into individual contributions from the present set of data. Although we have obtained numerical values of $\sigma$ in the range of $(1.0–3.0) \cdot 10^{-3}$ (Table I) and these are within the same range as reported,[13] they depend on the numerical value of the adapted $\Delta H$.

## Pressure Dependence of the Conformational Transition Temperature

Figure 4 shows the conformational transition temperature vs. the hydrostatic pressure in solution at solution ionic strengths of 10 and 25 m$M$. Despite the scatter in the data, there is a systematic decrease in $T_m$ when the hydrostatic pressure is increased. The slopes from Figure 4 estimated using linear regression are $(\Delta T_m/\Delta p) = -(9.5 \pm 4.0)\ 10^{-8}$ K Pa$^{-1}$ for $I$ = 10 m$M$ NaCl and $(\Delta T_m/\Delta p) = -(20 \pm 10)\ 10^{-8}$ K Pa$^{-1}$ for $I$ = 25 m$M$ NaCl. These numerical values are slightly more negative than those reported for the pressure dependence of the gelation temperature for $\kappa$- and $\iota$-carrageenans[10] and about 10 times more negative than those reported for the pressure dependence of the double-helical melting temperature of syntethic polyriboadenylic-polyribouridylic acid,[7] whereas it is opposite in sign and about five times as large in magnitude as that reported for DNA isolated from various sources.[7,30]

The observed pressure dependence of the melting temperature can be used to calculate an apparent change in the free volume between the ordered and disordered conformation using the Clausius–Clapeyron equation:

$$\left(\frac{\partial T_m}{\partial p}\right) = T_m \frac{\Delta V}{\Delta H} \qquad (7)$$

The volume change $\Delta V$ calculated from eq. (7) using the adopted literature value of $\Delta H$ = 7.1 kJ/mol for the order-to-disorder conformational transition yields $\Delta V = -(2.0 \pm 0.9)$ mL/mol at $I$ = 10 m$M$ NaCl and $\Delta V = -(4.0 \pm 2.0)$ mL/mol at $I$ = 25 m$M$. Although these $\Delta V$ values depend on the numerical value of $\Delta H$, they are both comparable in magnitude to values reported for other conformational transitions, such as for gelation of carrageenans where the volume change occurring in the crosslink formation is $\Delta V = 5 - 40$ mL/mol crosslinks.[10] Detailed interpretation of these thermodynamic results is outside the scope of this study because of the experimental limitations imposed by the upper pressure obtainable. However, a few comments on the sign of $(\Delta T_m/\Delta p)$ and $\Delta V$ will be offered since they are opposite to what is reported for the pressure dependence of DNA where hydrogen bonds are a major contributor to the stability of the double strand.

Formation of higher-ordered structures, e.g., double-strand formation in the case of DNA, are usually accompanied with a reduction of the free volume. The observed $\Delta V$ thus indicates an increase in free volume on going from the disordered to ordered conformation that most likely is due to differences in the hydration of the polymer in the two states. The $\Delta V$ consists of several contributions that are positive or negative depending on their origin. From X-ray fiber diffraction studies, only one potential interchain hydrogen bond was identified in the proposed antiparallel double-helical structure of xanthan, whereas four intrachain hydrogen bonds might exit.[31] If these hydrogen bonds are the major contributors to stabilizing the double-stranded ordered conformations of xanthan and these hydrogen

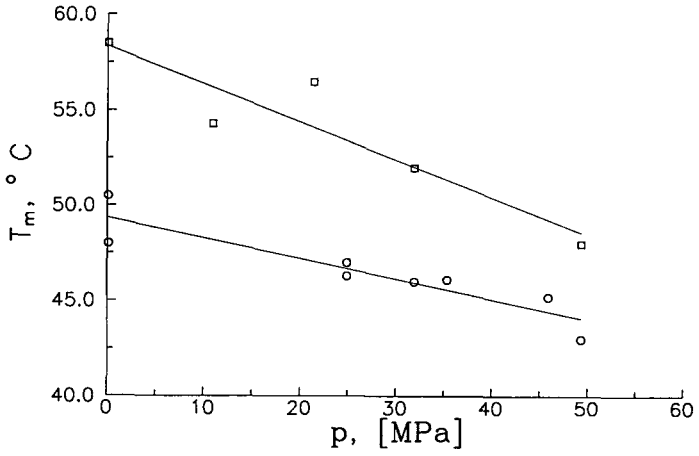


**Figure 4** Estimated conformational melting temperature of xanthan in dilute aqueous sodium chloride of 10 m$M$ (○) and 25 m$M$ (□) vs. hydrostatic pressure in solution.

bonds are partly replaced by polymer-solvent hydrogen bonds on going through the conformational transition, one would expect that elevated pressure increased the stability of the ordered conformation of xanthan similar to the pressure effect of the hydrogen-bond-stabilized DNA. The observed destabilization of xanthan may therefore suggest that there are other, i.e., hydrophobic or other effects, that dominate in stabilizing the ordered conformation of xanthan. The sensitivity of urea both on the specific optical rotation and rheological measurements led Frangou and co-workers[32] to the conclusion that hydrogen bonding is contributing to the intermolecular association, but other physical forces are also involved. Furthermore, increasing pressure is reported to destabilize ribonuclease A, and a negative $\Delta V$ was reported for this globular protein where hydrophobic forces are involved in the stabilization.[18] The sign of $\Delta T_m/\Delta p$ and $\Delta V$ reported herein for xanthan are therefore not at variance with existing molecular interpretations of the conformational transition of xanthan, and comparison with other studies[32] suggests that hydrophobic forces are involved.

## CONCLUDING REMARKS

This study shows that the conformational transition temperature of at least one type of xanthan decreases slightly as the hydrostatic pressure in solution is increased. For xanthan solutions used in high-temperature, high-salinity reservoirs, this lowering of the structural transition temperature is significant, but may not be a major limitation to the use of xanthan at these conditions. The largest shift in $T_m$ of xanthan for hydrostatic pressures up to 50 MPa is $< -10$ K relative $T_m$ at ambient pressure. For heavy brines such as saturated $CaCl_2/NaCl$, $T_m$ is estimated to be in the order of $> 130°C$.[2] A 10°C decrease in $T_m$ due to the high pressure will not lower $T_m$ sufficiently toward the temperature regions where it is assumed that xanthan is applicable, i.e., $< 90°C$. A possible pressure-induced change from the ordered to the inherently more thermally labile disordered conformation is therefore not the limiting factor in such applications.

However, if the operational conditions in the reservoir are such that the onset of the conformational transition is encountered at atmospheric pressure, the observed decrease in $T_m$ due to the high pressure is expected to have a significant effect on both the thermal and biological stability.

In addition to these applied perspectives, this study indicates that the volume change associated with the conformational transition is within that reported for sol-gel transitions of carrageenans. The present estimates of the thermodynamic parameters are, however, rather uncertain due to scatter in experimental determined values and because of the somewhat limited pressure range applied. More precise measurements are needed for detailed quantitative discussion of the thermodynamics of the conformational transition of xanthan.

This work was supported by grant St.10.12.220016 from the Royal Norwegian Council for Scientific and Industrial Research (NTNF), grant T. 6399 from Den norske stats oljeselskap a.s. (Statoil), and VISTA, a research cooperation between the Norwegian Academy of Science and Letters and Den norske stats oljeselskap a.s. (Statoil).

## REFERENCES

1. P. Davison and E. Mentzer, *Soc. Pet. Eng. J.*, **June,** 353–362 (1982).
2. R. S. Seright and B. J. Henrici, Soc. of Petroleum Eng. SPE/DOE 14946, presented at SPE/DOE 5th Symposium on Enhanced Oil Recovery, Tulsa, OK, April 20–23, 1986.
3. R. G. Ryles, *SPE Reservoir Eng.*, **February,** 23–34 (1988).
4. C. Kierulf and I. W. Sutherland, *Carbohydr. Polym.*, **9,** 185–194 (1988).
5. F. Lambert and M. Rinaudo, *Polymer,* **26,** 1549–1553 (1985).
6. P. Foss, B. T. Stokke, and O. Smidsrød, *Carbohydr. Polym.*, **7,** 421–433 (1987).
7. T. E. Gunter and K. K. Gunter, *Biopolymers,* **11,** 667–678 (1972).
8. I. W. Sutherland, *Carbohydr. Res.*, **131,** 93–104 (1984).
9. K. Suzuki, Y. Taniguchi, and T. Enomoto, *Bull. Chem. Soc. Jpn.*, **45,** 336–338 (1972).
10. K. Gekko and K. Kasuye, *Int. J. Biol. Macromol.*, **7,** 299–306 (1985).
11. S. Claesson and L. D. Hayward, *Chem. Scr.*, **9,** 18–20 (1976).
12. K. Knudsen, B. T. Stokke, A. Mikkelsen, and A. Elgsaeter, in *Construction of a Spectropolarimeter and a Low-Frequency Viscometer for Studies of Polymer Solutions at Elevated Temperature and Pressure,* K. Knudsen, dr.ing. thesis, The Norwegian Institute of Technology, University of Trondheim, Norway, 1989, pp. 4.1–4.20.
13. I. T. Norton, D. M. Goodall, S. A. Frangou, E. R. Morris, and D. A. Rees, *J. Mol. Biol.*, **175,** 371–394 (1984).
14. T. Igushi, S. Kitamura, and T. Kuge, *Makromol. Chem.*, **7,** 497–503 (1986).
15. F. V. Sander, *J. Biol. Chem.*, **148,** 311–319 (1943).

16. S. J. Gill and R. L. Glogovsky, *Rev. Sci. Instr.*, **35,** 1281–1283 (1964).
17. R. C. Weast, Ed., *Handbook of Chemistry and Physics,* CRC Press, Boca Raton, FL, Vol. 62, 1982, p. F-76.
18. S. J. Gill and R. L. Glogovsky, *J. Phys. Chem.*, **69,** 1515–1519 (1965).
19. M. Dubois, K. A. Gilles, J. K. Hamilton, P. A. Rebers, and F. Smith, *Anal. Chem.*, **28,** 350–356 (1956).
20. D. A. Rees, *Biochem. J.*, **126,** 257–273 (1972).
21. G. Holzwarth, *Biochemistry,* **15,** 4333–4339 (1976).
22. E. R. Morris, D. A. Rees, G. Young, M. D. Walkinshaw, and A. Darke, *J. Mol. Biol.*, **110,** 1–16 (1977).
23. H. Kitagawa, T. Sato, T. Norisuye, and H. Fujita, *Carbohydr. Polym.*, **5,** 407–422 (1985).
24. W. Liu, T. Sato, T. Norisuye, and H. Fujita, *Carbohydr. Res.*, **160,** 267–281 (1987).
25. E. S. Stevens and B. K. Sathyanarayana, *Carbohydr. Res.*, **166,** 181–193 (1987).
26. B. T. Stokke, A. Elgsaeter, and O. Smidsrød, in *Oil-Field Chemistry. Enhanced Recovery and Production Stimulation,* J. K. Borchardt and T. F. Yen, Eds., Am. Chem. Soc. Symp. Ser. 396, American Chemical Society, Washington, DC, (1989), pp. 145–156.
27. B. T. Stokke, O. Smidsrød, and A. Elgsaeter, *Biopolymers,* **28,** 617–637 (1989).
28. C. R. Cantor and P. R. Schimmel, *Biophysical Chemistry. Part III. The Behavior of Biological Macromolecules,* W. H. Freeman, San Francisco, 1980, Chap. 20.
29. M. S. Caceci and W. P. Cacheris, *Byte,* **May,** 340–362 (1984).
30. S. A. Hawley and R. M. Macleod, *Biopolymers,* **13,** 1417–1426 (1974).
31. K. Okuyama, S. Arnott, R. Moorhouse, D. Walkinshaw, E. D. T. Atkins, and Ch. Wolf-Ullish, Am. Chem. Soc. Symp. Ser. 141, American Chemical Society, Washington, DC, 1980, pp. 411–427.
32. S. A. Frangou, E. R. Morris, D. A. Rees, R. K. Richardson and S. B. Ross-Murphy, *J. Polym. Sci. Polym. Lett. Ed.*, **20,** 531–538 (1982).

*Received August 28, 1989*
*Accepted June 13, 1990*